




A comprehensive investigation on the role of PbO in the structural and radiation shielding attribute of $P_2O_5-CaO-Na_2O-K_2O-PbO$ glass system

Nuha Al-Harbi^{1,2}, M. I. Sayyed^{3,4,*} , Ashok Kumar^{5,6}, K. A. Mahmoud^{7,8}, O. I. Olarinoye⁹, Abdullah M. S. Alhuthali¹⁰, and Yas Al-Hadeethi¹

¹Department of Physics, Faculty of Science, King Abdulaziz University, Jeddah 21589, Saudi Arabia

²Department of Physics, Umm AL-Qura University, Makkah, Saudi Arabia

³Department of Physics, Faculty of Science, Isra University, Amman, Jordan

⁴Department of Nuclear Medicine Research, Institute for Research and Medical Consultations (IRMC), Imam Abdulrahman bin Faisal University (IAU), PO Box 1982, Dammam 31441, Saudi Arabia

⁵University College, Benra- Dhuri, Punjab, India

⁶Department of Physics, Punjabi University, Patiala, Punjab, India

⁷Ural Federal University, St. Mira, 19, 620002 Yekaterinburg, Russia

⁸Nuclear Materials Authority, Maadi, Cairo, Egypt

⁹Department of Physics, Federal University of Technology, Minna, Nigeria

¹⁰Department of Physics College of Sciences, Taif University, PO Box 11099, Taif 21944, Saudi Arabia

Received: 12 February 2021

Accepted: 29 March 2021

Published online:
20 April 2021

© The Author(s), under exclusive licence to Springer Science+Business Media, LLC, part of Springer Nature 2021

ABSTRACT

This study presents the synthesis, physical, structural and gamma-ray shielding characteristics of $40P_2O_5-20CaO-(30-x)Na_2O-10K_2O-xPbO$ ($x = 0, 5, 10, 15, 20$ mol%) glasses. The glass samples coded as PbCKNP1, PbCKNP2, PbCKNP3, PbCKNP4, and PbCKNP5 were prepared using the melt quench method. Na_2O substitution by PbO influenced the molar volume and mass density of the glasses. Structural analysis of the glasses using the X-ray diffraction (XRD) and Fourier transform infrared (FTIR) spectroscopy confirmed amorphous structure. The photon shielding parameters of the glasses examined via the Monte Carlo simulation code (MCNP-5) revealed that the glasses' shielding ability improved as PbO content increased. The highest simulated linear attenuation coefficient (LAC) achieved at 0.015 MeV increased from 21.46 to 159.07 cm^{-1} as the PbO concentration increased from 0 and 20 mol%. The LAC for all fabricated glass samples showed an exponential reduction trend with gamma photon energy. Based on the simulated LAC values, calculated mass attenuation coefficient (MAC), half-value layer (HVL), transmission factor (TF), and radiation shielding capacity (RSC), PbCKNP5 possessed the best gamma-ray protection ability among the investigated glasses. Furthermore, the calculated shielding

Address correspondence to E-mail: mabualssayed@ut.edu.sa

parameters of the PbCKNP glasses showed that they possess a good potential for radiation shielding applications.

1 Introduction

Radiations (neutrons, electrons, charged heavy particles, x- and gamma-rays) with sufficiently high energies are important tools in modern technology that have made life on earth more comfortable and enduring. Notable among the areas in which these radiations are applied for the general benefit of man and his environment include: in the diagnosis and management of health impairments, power generation, non-destructive testing, and industrial processes, research, material characterization, environmental conservation, food cultivation, processing, and preservation [1–7]. These application frontiers continue to soar despite the enormous hazards associated with exposure to all forms of artificial radiation sources. This is because such risks have been successfully brought to the barest minimum and eliminated in some cases through the availability of adequate radiation control measures.

Radiation control is efficient when good radiation dosimetry and shielding systems are in place in all radiation facilities. Radiation interaction parameters are crucial for determining the chosen material for radiation shielding analysis and design as they provide information about the amount of radiation and energy absorbed by different materials. Hence, interaction parameters can be processed to provide information about a material's competence to provide radiation protection in nuclear facilities. Furthermore, they are used to quantify the comparative advantage a material has over existing radiation shields. Many functional materials such as steel, alloys, ceramics, metallic, and glasses have been investigated for their radiation shielding competence via analysis of various radiation interaction parameters [8–15]. Many of these materials have shown great potential, similar and sometimes superior to lead (Pb) and concretes two traditional shielding materials. The demand to replace these two basic shields has increased in recent years due to non-homogeneity and stability of chemical components, presence of crack and pores in concrete, opacity, high density, and environmental issues associated with Pb.

Today, many oxide glasses possessing diverse structural, mechanical and chemical characterization have been investigated for their radiation shielding efficiency against different radiations. This is possibly due to their comparatively better chemical and mechanical stability relative to other glasses [16, 17]. Phosphate glasses have the ability to host a high concentration of transition metals in their amorphous state [17]. Their unique chemical structure and composition flexibility enable one to alter their chemical composition, thus allowing the tailoring of their structural, physical, and chemical properties to any desired state for several applications easier.

For the purpose of radiation shielding, the addition of PbO into glass systems has been reported to enhance the photon and charged particle shielding competence of such glasses [18–21]. The high atomic number and density of Pb have been concluded to be responsible for this. The effect of different amounts of PbO in the nuclear shielding competence of the $\text{Na}_2\text{O}_5\text{-BaO-PbO-Nb}_2\text{O}_5\text{-SiO}_2\text{-Al}_2\text{O}_3$ ceramic system was investigated previously [18]. Via the Geant4 simulation tool's use, the gamma and heavily charged particle absorption capacity of the ceramics were found to be superior for those with higher PbO content. Similar increases in radiation shielding ability with higher PbO content have been reported for different glass systems by Aly et al. [19] and Alalawi et al. [20]. Also, Kavaz et al. [21] discovered that mass density increased, and molar volume decreased while the optical, photon, and the neutron-absorbing tendency of $\text{V}_2\text{O}_5\text{-SrO-PbO}$ glasses improved with an increase in their PbO content.

Subsequently, phosphate glasses with a certain level of PbO content could potentially be a good radiation shield that might be used to construct containers for storing and transporting nuclear waste. They could also be used as radiation shields in nuclear facilities where high-energy photons and charged particles are utilized. The addition of PbO encourages the formation of Pb–O–P chemical bonds, which is expected to improve the chemical stability significantly and the amorphous state, among other benefits in phosphate glass systems [22]. Such chemical structure enhancement has also been

reported to improve physical properties [23]. Above all, the environmental toxicity concern of the Pb shield can be drastically reduced since Pb is oxidized and reacts with the phosphate glass network. The Pb in such a network can only be freed via extreme physicochemical processes [24] thus, preventing it from becoming a contaminant in the environment. Phosphate glass systems containing PbO could be subsequently safe and potentially effective radiation absorbers. However, this assertion requires a quantitative investigation as radiation shielding ability depends on the nature and energy of the radiation, chemical composition, and state of the absorbing material. Furthermore, the structural, mechanical, chemical and other properties of glass shields determine how they could be deployed for a shielding function and dictate the nature of the environment they can be deployed for such functionality.

The novelty of the present work comes from the fabrication of a glass series consisting of five glass samples. The chemical composition of the fabricated glass samples described by the chemical formula $x\text{PbO} + 20\text{CaO} + 10\text{K}_2\text{O} + (30-x)\text{Na}_2\text{O} + 40\text{P}_2\text{O}_5$, x take values 0, 5, 10, 15, and 20 mol%. The structure and physical properties were studied experimentally for the fabricated glass samples. Moreover, the Monte Carlo simulation code (MCNP-5) was used to evaluate the radiation shielding parameters, while the XCOM database was used to confirm the simulated shielding parameters.

2 Materials and methods

2.1 Preparation of samples

The glass samples of the selected glass composition of $40\text{P}_2\text{O}_5-20\text{CaO}-(30-x)\text{Na}_2\text{O}-10\text{K}_2\text{O}-x\text{PbO}$ and ($x = 0, 5, 10, 15, 20$ mol%) were prepared using the method of melt quenching technique. The initial chemicals are taken as P_2O_5 , CaCO_3 , PbO , NaOH , and KOH in the stoichiometric amount, and also analytic grade chemicals were used to prepare the selected glass composition. In this glass composition, lead oxide was added of different molar percentages (x mol%) where $x = 0, 5, 10, 15$, and 20 mol% to make the mixtures. The selected chemicals were mixed thoroughly, and the mixture was melted at 1050°C in an electrical furnace. The melt was poured into pre-heated graphite molds. The samples were annealed

in an annealing furnace at 320°C for 2 h and then slowly cooled to room temperature for 24 h to reduce the selected glass samples' cracking and thermal strain. The detailed procedure has already been explained in our previous findings [25, 26]. The picture of prepared glass samples is displayed in Fig. 1. Each prepared glass samples' density was measured using the Archimedes' principle [27, 28]. The densities increase from 2.3337 to 3.5431 g/cm^3 as the mol% of the PbO increases, which is listed in Table 1. The prepared glass samples were subjected to structural characterizations via XRD and FTIR spectroscopy.

2.2 Structural characterization

XPRT-PRO XRD system was used to determine the amorphous phase of the selected powdered glasses. The voltage and current values of 45 kV and 40 mA were used, respectively. The analysis was conducted with Cu (K-alpha wavelength) and approximately equal to 1.54 \AA with 2θ varying from 20° to 80° with a step size of 0.02 .

The FTIR spectra of the selected glass samples in the spectral range $1600-400\text{ cm}^{-1}$ were obtained with PE-IR sub-tech spectrum ASCII FTIR Spectrophotometer. The fine mixture was mixed with potassium bromide (KBr), and the mixed mixture was pressed in a hydraulic press. FTIR spectra were obtained to study the structural variations present in the selected glass samples.

2.3 Gamma-ray shielding and geometry setting

Due to the dangerous effect of radioactive sources, their wrong use and handling, many research works have reported the shielding properties of different shielding materials by means of theoretical calculations as alternative methods for the experimental measurements. Monte Carlo N-Particle transport code is a useful creative code able to estimate the gamma photons' average track length per unit shielding material. An accurate arranged input file is required to obtain precise simulated shielding parameters. The organized geometry is illustrated in Fig. 2. As shown in the geometry described in Fig. 2, the radioactive source existed in the center of the geometry. A lead collimator surrounds the

Fig. 1 Picture of the prepared samples

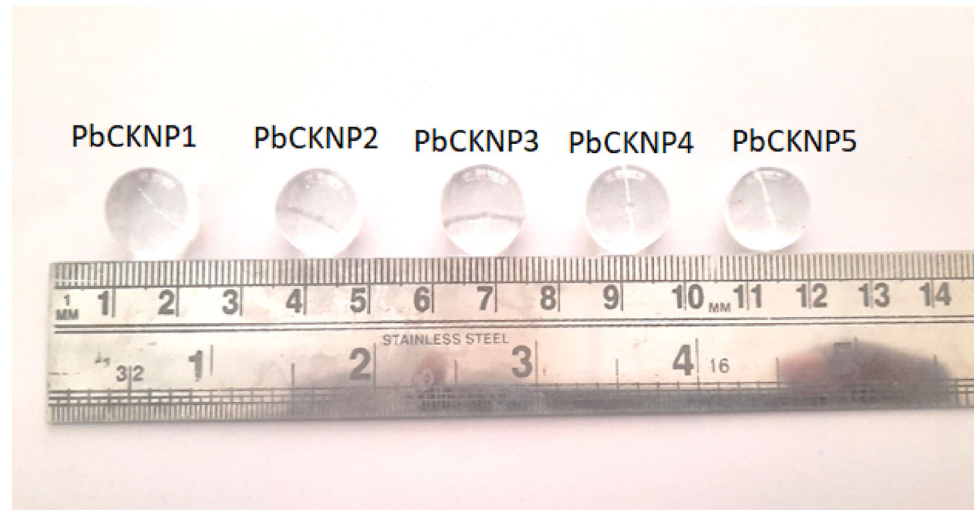


Table 1 Chemical composition and density of PbCKNP glass samples

Glass code	Glass composition (mol%)					Density (g/cm^3)
	PbO	CaO	K ₂ O	Na ₂ O	P ₂ O ₅	
PbCKNP1	0	20	10	30	40	2.3337
PbCKNP2	5	20	10	25	40	2.8930
PbCKNP3	10	20	10	20	40	3.1726
PbCKNP4	15	20	10	15	40	3.4531
PbCKNP5	20	20	10	10	40	3.7431

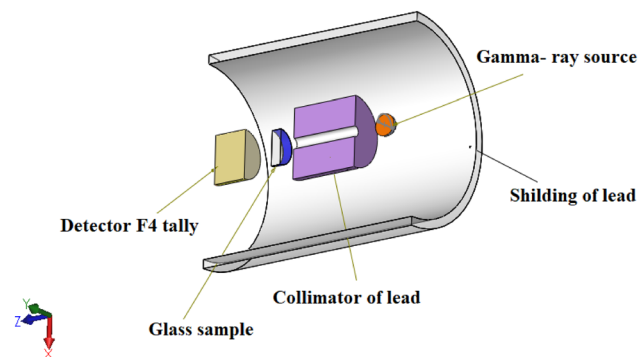


Fig. 2 The MCNP geometry used in the radiometric study

radioactive source with a vertical slit of 1 cm diameter. The collimator was used to collimate the incident photons and directed them along the Z direction. Figure 2 also shows that the fabricated glass sample was between the collimator and the detector. The fabricated glass samples' chemical composition, dimensions, and density were introduced to the input file in the parts related to material,

surface, and cell cards. The detector was located at a distance of 10 cm from the collimator. The detector type was chosen to be an F4 tally. Thus, it can estimate the mean flux per unit cell of the detector. The MCNP-5 code was reached with the cross-section nuclear databases ENDF/B-VI.8, ACTI, ENDL, ACTI, and T-16 files. The NPS card is arranged to be 10^6 histories [29].

The simulated results were confirmed using the XCOM database program. Moreover, based on the gamma-flux simulated mean track length, the linear attenuation coefficient (LAC) was calculated. After that, the mass attenuation coefficient (MAC), half-value thickness ($\Delta_{0.5}$), transmission factor (TF), and radiation shielding capacity (RSC) were evaluated using standard expressions.

3 Results and discussion

3.1 Glass physical and structural characterization

The fabricated glasses' density (ρ , g/cm^3) was determined experimentally using the Archimedes method with a standard uncertainty of $\pm 0.01 \text{ g}/\text{cm}^3$. After that, the molar volume (V_M , cm^3/mol) was calculated based on the fabricated glass samples' measured density and molecular weight. The obtained values for ρ and V_M were plotted versus the PbO content, as presented in Fig. 3. Figure 3 depicts that the ρ (g/cm^3) was enhanced with rising PbO in the fabricated glass system. The density takes values 2.334, 2.893, 3.173, 3.453, and 3.743 g/cm^3 for glass

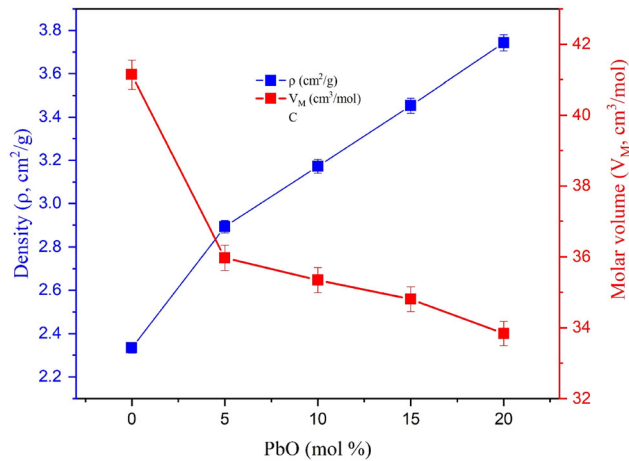


Fig. 3 Variation of the glass density and molar volume versus the PbO insertion ratio

samples with PbO concentration 0, 5, 10, 15, and 20 mol%, respectively. In contrast, the V_M decreased in order 41.14, 35.972, 35.34, 34.81, and 33.83 cm³/mol with raising the PbO concentrations. This increase in density is due to the replacement of Na₂O contents ($\rho = 2.27$ g/cm³ and $M_w = 61.97$ g/mol) by PbO content ($\rho = 9.53$ g/cm³ and $M_w = 223.2$ g/mol). The drastic influence over density by the first 5% of PbO addition to the base material which may be due to the effect of other modifiers present in the glass network. These modifiers also play important role to change the structure of glass which directly affect the density of the glasses.

The X-ray diffraction spectra of selected samples have been recorded and shown in Fig. 4. It shows no sharp peaks, but there is only one hump representing the selected samples having an amorphous structure.

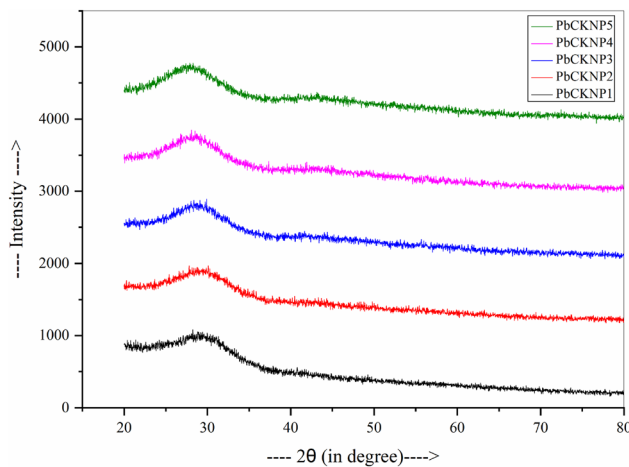


Fig. 4 The XRD spectra of the present glasses

So, it is cleared that all the presented samples are glassy materials of the order of amorphous structures.

The Fourier transformation infrared (FTIR) spectra recorded is displayed for all the selected glasses in Fig. 5. The various peaks and their assignments of recorded FTIR spectra are represented in Table 2. There are various modes of vibrations and linkages present in the selected glass samples. The IR transmission spectra of investigated glasses have main bands at around ~ 510 cm⁻¹, ~ 710 cm⁻¹, ~ 880 cm⁻¹, ~ 1100 cm⁻¹, ~ 1240 cm⁻¹, and ~ 1366 cm⁻¹. A strong peak of FTIR recorded at 510 cm⁻¹ is attributed to the Pb–O symmetrical bending vibration, Pb–O bending of PbO₄ groups, and bending vibrations of bridging phosphorus δ (O–P–O) [20–32]. A peak is observed at 710 cm⁻¹, which reveals the covalent bond between non-bridging oxygen and calcium ions as P–O–Ca stretching vibrations [30]. P–O–P groups’ asymmetric stretching vibration linked with linear metaphosphate chain is observed at the peak position 880 cm⁻¹ [30]. The IR peaks at 1100 cm⁻¹ may be due to Pb–O asymmetrical bending vibration as well as asymmetric stretching of P–O–P groups [31, 33]. A peak around 1240 cm⁻¹ and 1366 cm⁻¹ is attributed to the asymmetric and symmetric stretching vibration (P=O), respectively [30, 34]. The first band around 400–650 cm⁻¹ reveals the Pb–O symmetrical bending vibrations [31, 32]. The second band around 650–800 cm⁻¹ is due to the symmetric stretching vibrations of P–O–P linkages in rings [30]. Around 800–1200 cm⁻¹, the third band is assigned to the symmetric, asymmetric stretching vibration of P–O–P linkages. The last band around 1200–1400 cm⁻¹

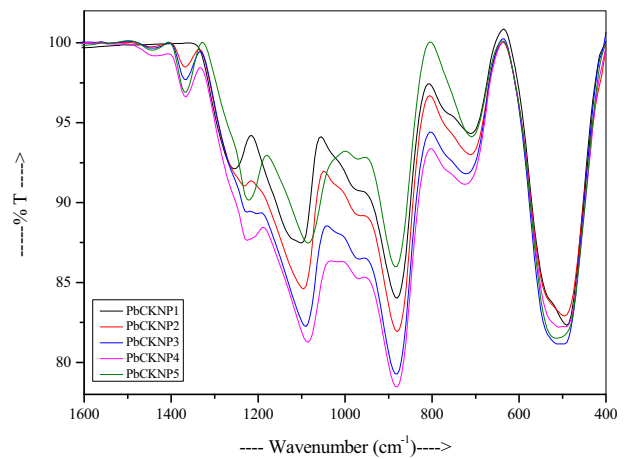


Fig. 5 The FTIR spectra of the present glasses

Table 2 The mass attenuation coefficient of the fabricated PbCKP glass samples

Energy (MeV)	Mass attenuation coefficient (cm ² /g)																								
	PbCKP1					PbCKP2					PbCKP3					PbCKP4					PbCKP5				
	MCNP- 5	XCOM	Δ (%)	MCNP- 5	XCOM	Δ (%)	MCNP- 5	XCOM	Δ (%)	MCNP- 5	XCOM	Δ (%)	MCNP- 5	XCOM	Δ (%)	MCNP- 5	XCOM	Δ (%)	MCNP- 5	XCOM	Δ (%)	MCNP- 5	XCOM	Δ (%)	
0.015	9.1958	9.1930	0.0300	19.4564	19.4800	- 0.1214	28.2411	28.3000	- 0.2086	35.8485	35.9300	- 0.2274	42.4992	42.6000	- 0.2373										
0.03	1.3252	1.3240	0.0876	4.2217	4.2240	- 0.0552	6.7017	6.7070	- 0.0798	8.8491	8.8560	- 0.0782	10.7262	10.7400	- 0.1284										
0.05	0.4157	0.4154	0.0723	1.1737	1.1780	- 0.3677	1.8227	1.8300	- 0.4007	2.3847	2.3950	- 0.4330	2.8759	2.8890	- 0.4560										
0.08	0.2156	0.2155	0.0361	0.4308	0.4357	- 1.1271	0.6152	0.6242	- 1.4685	0.7748	0.7875	- 1.6453	0.9143	0.9302	- 1.7391										
0.3	0.1064	0.1065	- 0.1364	0.1358	0.1361	- 0.2337	0.1610	0.1614	- 0.2609	0.1828	0.1834	- 0.3335	0.2030	0.2026	0.1781										
0.5	0.0861	0.0862	- 0.0851	0.0936	0.0938	- 0.1882	0.0999	0.1002	- 0.2576	0.1055	0.1058	- 0.3255	0.1103	0.1107	- 0.3831										
0.8	0.0697	0.0698	- 0.0905	0.0716	0.0717	- 0.1689	0.0732	0.0734	- 0.2157	0.0746	0.0748	- 0.2694	0.0758	0.0761	- 0.3141										
1	0.0625	0.0627	- 0.3335	0.0631	0.0636	- 0.7875	0.0636	0.0643	- 1.1630	0.0640	0.0650	- 1.4815	0.0644	0.0655	- 1.7566										
1.5	0.0509	0.0511	- 0.3137	0.0509	0.0512	- 0.5772	0.0509	0.0514	- 0.7861	0.0510	0.0515	- 0.9796	0.0510	0.0516	- 1.1364										
3	0.0359	0.0360	- 0.3118	0.0365	0.0367	- 0.4024	0.0370	0.0372	- 0.4660	0.0375	0.0377	- 0.5336	0.0379	0.0381	- 0.5679										
5	0.0286	0.0287	- 0.2640	0.0300	0.0301	- 0.2763	0.0312	0.0313	- 0.2931	0.0322	0.0324	- 0.3181	0.0332	0.0333	- 0.3200										
8	0.0243	0.0244	- 0.2400	0.0266	0.0266	- 0.2289	0.0285	0.0286	- 0.2310	0.0302	0.0302	- 0.2313	0.0316	0.0317	- 0.2313										
10	0.0230	0.0231	- 0.2479	0.0257	0.0258	- 0.2360	0.0280	0.0281	- 0.2045	0.0300	0.0301	- 0.2138	0.0317	0.0318	- 0.1869										
15	0.0216	0.0217	- 0.2358	0.0251	0.0252	- 0.2144	0.0281	0.0282	- 0.1774	0.0307	0.0308	- 0.1651	0.0330	0.0330	- 0.1743										

is assigned to the stretching vibration of doubly bonded oxygen, respectively [34, 35]. We know that as lead doping increases the bond between lead and oxygen becomes weaker which indicates the increase in number of the non-bridging oxygen. So we can say that, Pb–O bond become more dominating as lead increases than Pb=O bond. This is the reason why we get very small kinks at 1240 and 1360 cm^{-1} .

3.2 Evaluation of the radiation shielding capacity

The average track length simulated using the Monte Carlo N-particle Transport code-version 5 (MCNP-5) was used to estimate the synthesized glass samples' LAC values in the energy range between $0.015 \leq E \leq 15$ MeV. Figure 6 clarifies the LAC variation along the various energy spectrum regions (low, mid, and high). It is clear the LAC takes its maximum values at gamma-ray energy 0.015 MeV, concerning the studied energy range. The highest LAC values were 21.460, 56.287, 89.597, 123.788, and 159.078 cm^{-1} for glass samples PbCKNP1, PbCKNP2, PbCKNP3, PbCKNP4, and PbCKNP5, respectively. This is due to the predominance of photo-electric interaction (PE). After that, the LAC values for all fabricated glass samples were highly diminished with rising incident gamma photon energy. The decreasing trend is due to the decreasing of the PE interaction with rising incident gamma energy in the

low energy interval between 0.15 and 0.15 MeV. In the energy interval between 0.08 and 0.1 MeV, an increase in LAC value was observed for all samples. This increase is attributed to the K-absorption edges of lead Pb at 0.088 MeV. Above 0.15 MeV, the Compton scattering interaction (CS) regularly increased with energy to 1.5 MeV. Thus, the LAC values in this interval decreased linearly with gamma photon energy. In the mentioned energy region between 0.15 and 1.5 MeV, the LAC value decreases from 0.330 to 0.118 cm^{-1} and from 3.061 to 0.190 cm^{-1} for glass samples PbCKNP1 and PbCKNP5 glass, respectively. This linear decrease is due to the CS cross-section where the $\sigma_{CS} \propto E^{-1}$. Figure 7 depicts that above gamma photon energy 2 MeV, the fabricated glass samples' LAC is nearly constant and independent of the incident photon energy. This is attributed to the pair production interaction (PP), where the $\sigma_{PP} \propto \log(E)$.

Figure 7 shows the PbO influence on the fabricated glass samples' LAC values at some fixed energy. Replacement of the NaO_2 with PbO content causes an enhancement in the fabricated glasses' molecular weight and density. Thus, the atomic number (Z) of the fabricated glass samples increased. Since the gamma-ray interaction cross-section varied with Z^{4-5} for photo-electric, the LAC values were observed to rapidly improve with rising the PbO content in the PE interaction region (i.e., 0.015 MeV). On the other hand, the LAC values were slightly increased with the PbO content in the Compton scattering and pair production interaction regions (i.e., 1 and 15 MeV)

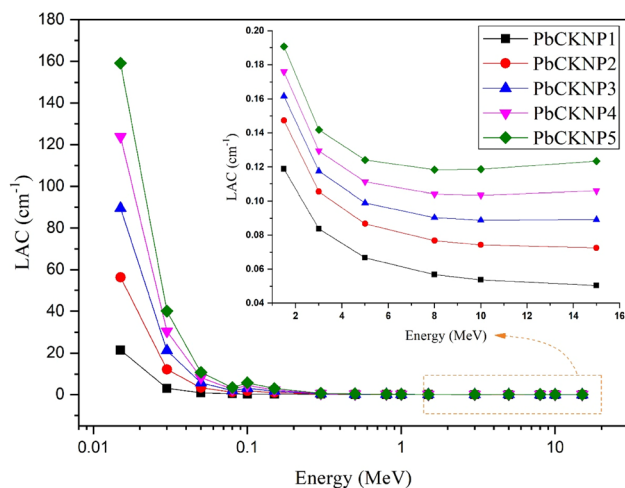


Fig. 6 The LAC (μ , cm^{-1}) of the PbCKNP glass series, as a function of the gamma-ray energy

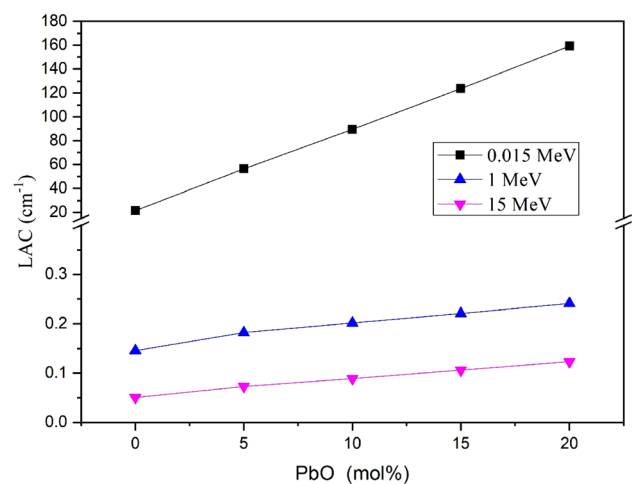


Fig. 7 The variation of the LAC (μ , cm^{-1}) of the PbCKNP versus the PbO content

due to the variation of the cross-section with Z and Z^2 of the fabricated glass samples.

The mass attenuation coefficient (MAC) was calculated for the present glass samples to ignore the density effect and estimate the attenuation coefficient per unit mass. The MAC (μ_m , cm^2/g) was calculated theoretically using the XCOM database and simulated using the MCNP-5 code, as shown in Table 3. Table 3 indicates that the simulated μ_m highest values are 9.195, 19.456, 28.241, 35.840, and 42.499 cm^2/g , while the lowest are 0.0216, 0.0251, 0.0281, 0.0307 cm^2/g , for glass samples PbCKNP1, PbCKNP2, PbCKNP3, PbCKNP4, and PbCKNP5, respectively. The simulated μ_m was comparable to the theoretically calculated using the XCOM database. The difference (Δ , %) between the simulated and XCOM results is calculated and plotted in Fig. 8. The Δ (%) presented in Fig. 8 was in the range $\pm 2\%$. This Δ (%) may be related to the different cross-section databases used by XCOM (NIST) and MCNP-5 code (ENDF/B-VI.8).

The half-value layer (HVL) is a potential shielding parameter used to describe the shielding material thickness to reduce incident photons' intensity to half. It is inversely proportional to the LAC. Thus, Fig. 9 depicts that the HVL increases with the incoming energy. The lowest HVL values were achieved at 0.015 MeV. their values are 0.0322, 0.0123, 0.0077, 0.0055, and 0.0043 cm for glass sample PbCKNP1, PbCKNP2, PbCKNP3, PbCKNP4, and PbCKNP5, as illustrated in subfigure 9. The HVL values were exponentially progressed with energy

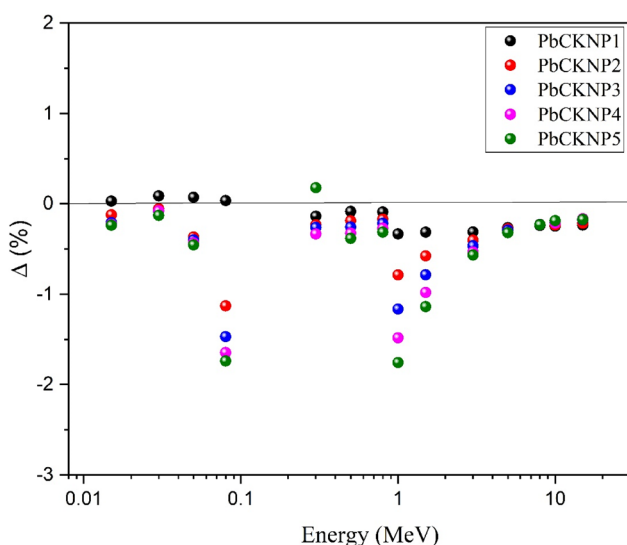


Fig. 8 Variation of the difference ($\Delta\%$) as a function of the gamma-ray energy

due to the PE interaction in the low energy region. Due to the CS cross-section, the HVL trend transformed to a linear increase with the mid-energy interval incident energy. The thinner HVL values were achieved at 0.015 MeV. They are 0.0323, 0.01231, 0.00774, 0.0056, and 0.00436 cm. In contrast, the highest HVL values were achieved at high energy (i.e., 10 MeV); they take values of 12.895, 9.319, 7.802, 6.694, and 5.837 cm for glass samples PbCKNP1, PbCKNP2, PbCKNP3, PbCKNP4, and PbCKNP5. At energy 10 MeV (for example), with increasing the PbO increased in order 5, 10, 15, 20 mol%, the HVL enhanced by factors 27.73, 39.49, 48.08, 54.72% for glass samples PbCKNP2, PbCKNP3, PbCKNP4, and PbCKNP5.

Also, the effect of glass composition appears brightly in Fig. 9, where the HVL is reduced gradually with increasing the PbO concentration in the fabricated glass. This effect also varies from one type of photon interaction to another. One can see that HVL values are highly dependent on the chemical composition of the material in the PE interaction region, where the cross-section of interaction varies with Z^{4-5} . While this effect decreased for CS and PP, where the cross-section varied with Z , and Z^2 , respectively. The lowest HVL was obtained for the PbCKNP1 glass sample. It increased from 0.032 to 13.75 while the thinner achieved for PbCKNP1 and increased from 0.004 to 5.61 cm, increasing energy between 0.015 and 15 MeV, respectively.

The transmission factor (TF) describes the photon ratio transmitted through a known thickness of the fabricated glass samples. Figure 10 depicts that

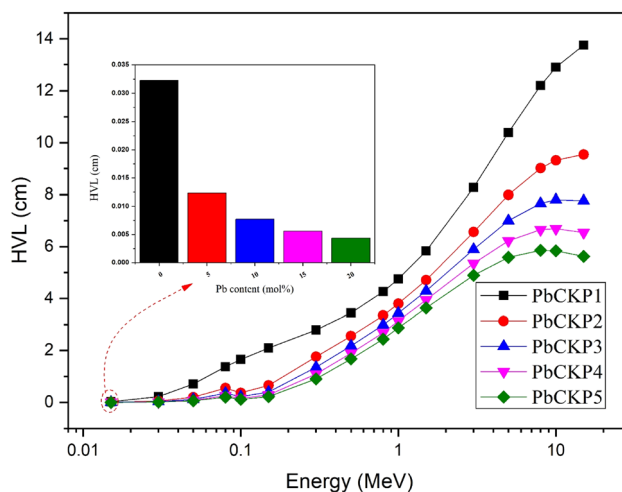


Fig. 9 The half-value layer (HVL) of the fabricated glass samples

photons’ transmission depends mainly on three factors, incident energy, chemical composition, and shielding thickness.

Figure 10 shows that the transmission factor at low energy (i.e., 0.08 MeV) decreases exponentially with PbO content; this is attributed to the PE interaction where the $\sigma_{PE} \propto Z^{4-5}$, as mentioned in the LAC section. For example, a glass sample with a thickness of 2 cm has the ability to reduce the incident intensity with ratios 63.439, 91.732, 97.982, 99.525, and 99.893% when the PbO content increased in order 0, 5, 10, 15, and 20 mol% at 0.08 MeV, respectively. Increasing the PbO content in the fabricated glass samples leads to additional resistance for the passing photons. Thus, the transmission factor decreased with increasing the PbO content. This decreasing trend depended mainly on the Z of the fabricated glass. So, as mentioned early, the TF was exponentially reduced with the PbO composition in the low energy region (i.e., 0.08 MeV). It linearly decreases in the mid and high energy

region, the CS and PP cross-section, which is proportional to Z and Z^2 , respectively. For example, the glass with the same previous thickness (2 cm) can reduce the intensity by a factor of 25.30, 30.58, 33.20, 35.73, and 38.25% with increasing the PbO ratio between 0, 5, 10, 15, and 20 mol% at 1 MeV, respectively.

The transmission factor is also affected by the gamma photon energy, as shown in Fig. 10a–c. The TF for a thickness of 1 cm from glass sample PbCKP5, as an example, increases in the order of 3.263, 78.589, and 88.386%, for gamma-ray energy 0.08, 1, and 15 MeV, respectively. Raising the incoming photon energy leads to a decrease in the gamma-photon wavelength. Thus, the penetration power of the projected photons increased. As a result, the gamma photons spend fewer scattering events while passing the shielding material thickness. A small number of interactions between the shielding material atoms and gamma photons took place. Thus, the material

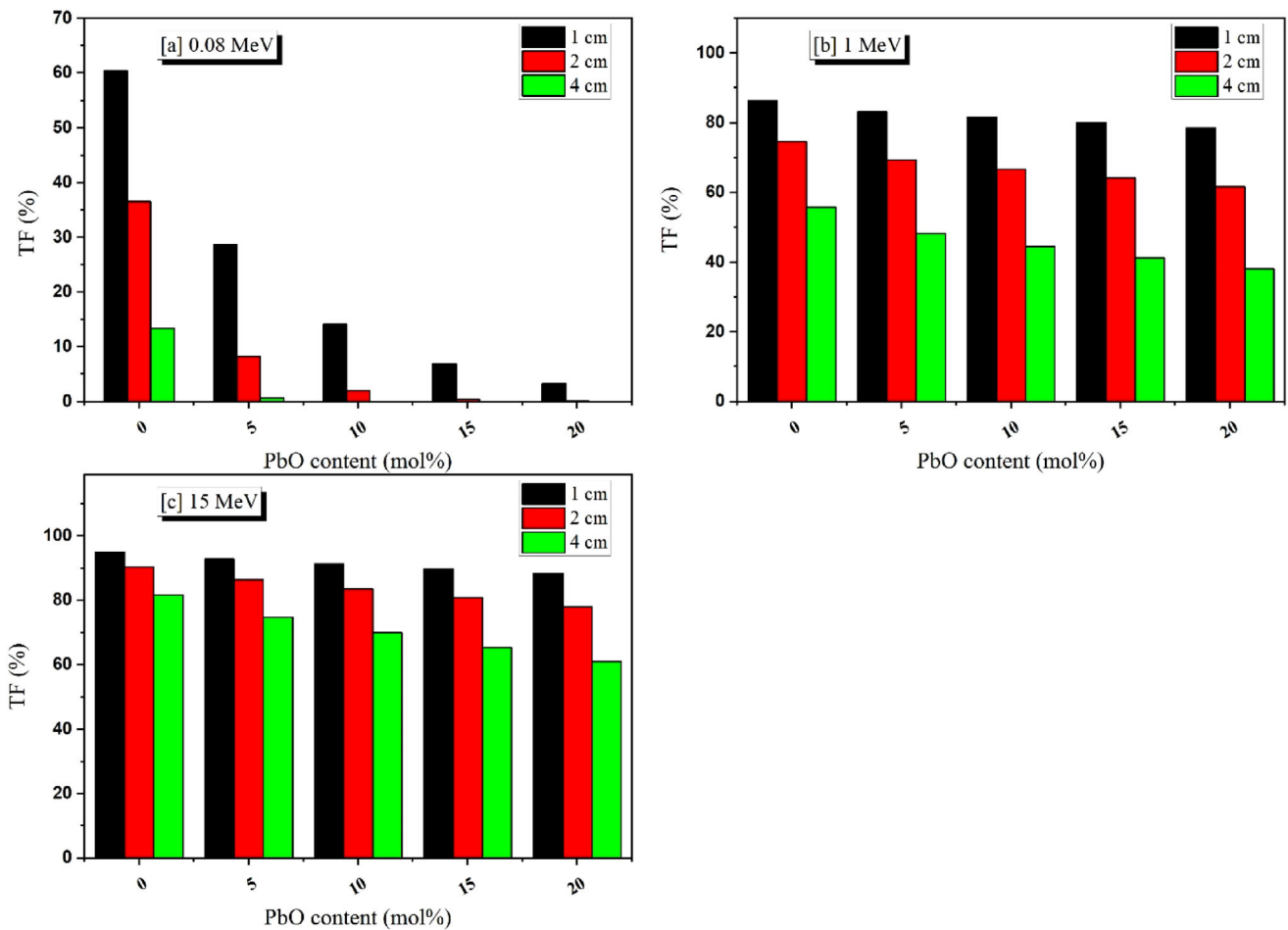


Fig. 10 The variation of the transmission factor as a function of the PbO content

resistance to the passing photons decreased, and the TF increased with gamma photon energy.

The radiation shielding capacity (RSC) is a measure of the investigated shielding material's protection, and it is inversely proportional to the transmission factor (TF). Thus, the materials with a high gamma-ray TF are not suitable for protection against gamma-photons. In contrast, the materials with a lower TF are an excellent selection for protection against gamma-photons. Figure 11 shows the variation of the RSC for the fabricated glass samples versus the glass thickness at some fixed gamma photon energies (0.08, 1, 15 MeV). The selected gamma-ray energies cover all the gamma-ray interaction types (PE, CS, and PP). Figure 11a–c show that the RSC increases gradually with the material thickness. Thus, the thicker glass

samples have better RCS than the thinner thicknesses. For example, the RSC of 4 cm thickness of glass PbCKP5 enhanced from 21.41 to 61.67%, increasing the glass thickness from 0.5 to 4 cm. This means that the RSC was improved by 34.7% when the glass thickness increased from 0.5 to 4 cm.

Also, the mentioned figure illustrates that the RCS level decreased gradually with raising the gamma photon energy. This decrease is related to the high penetration power which the high-energy photons received. Photons with high penetration power can penetrate the material thickness speedily with a few collisions number. Thus, the RSC decreased with raising the gamma-photon energy. For example, The RSC values offered by 2 cm thickness of the fabricated glass sample PbCKP5 are 99.89, 38.25, and 21.87

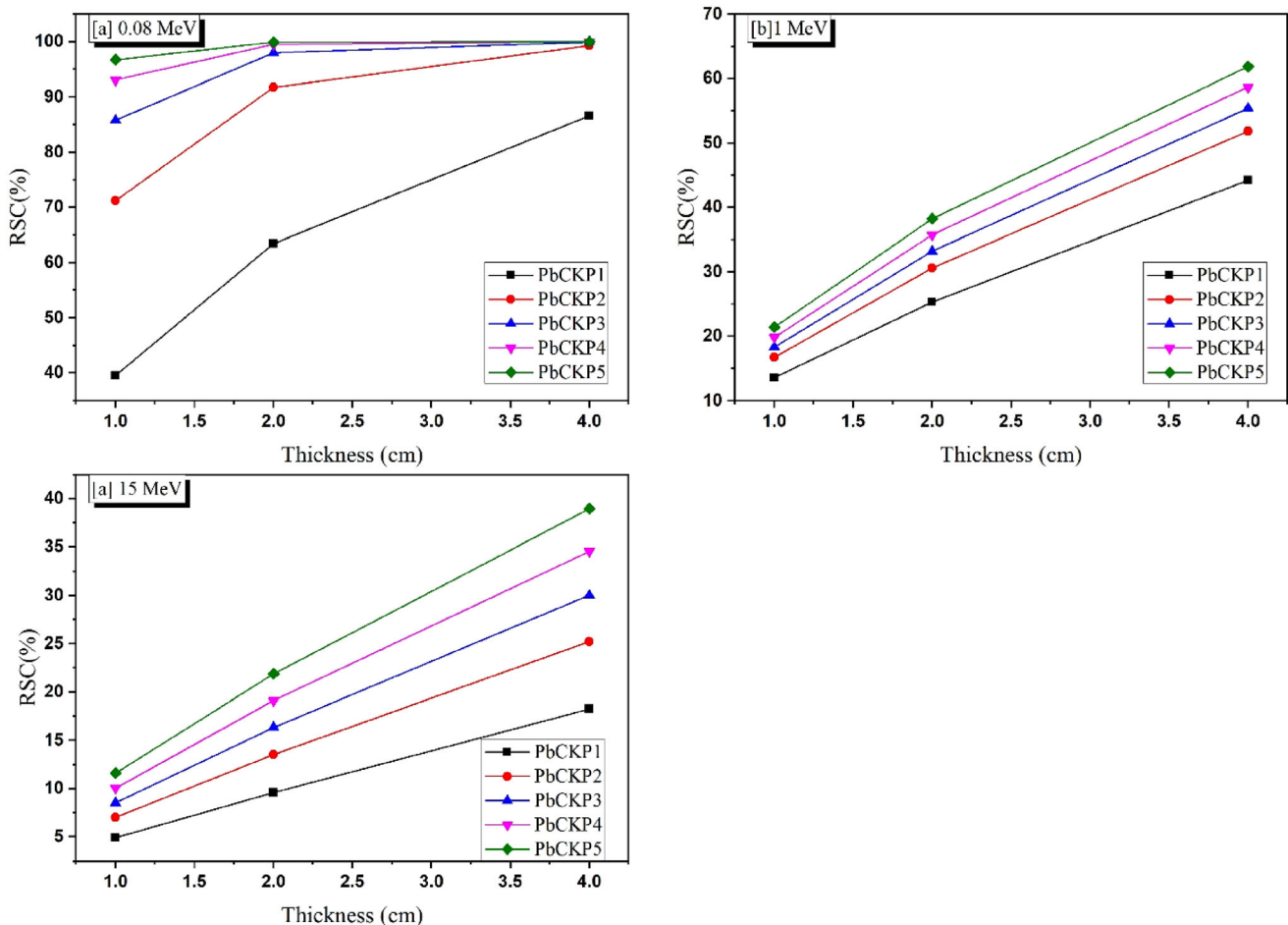


Fig. 11 Variation of the radiation shielding capacity (RSC, %) as a function of the glass thickness

when the gamma photon energy increased between 0.08, 1, and 15 MeV, respectively.

4 Conclusion

The structural characterization of synthesized glasses $40\text{P}_2\text{O}_5-20\text{CaO}-(30-x)\text{Na}_2\text{O}-10\text{K}_2\text{O}-x\text{PbO}$ and ($x = 0, 5, 10, 15, 20$ mol%) was studied using the X-ray and Fourier transform infrared spectroscopy. The density (ρ) and molar volume (V_M) of the fabricated glass samples were evaluated. The glass density increased from 2.333 to 3.743 g/cm³, while the V_M decreased from 41.139 to 33.832 cm³/mol, increasing the PbO concentration between 0 and 20 mol%, respectively. The absence of any sharp peak in XRD spectra indicates that samples were amorphous in nature. The FTIR spectra showed the various modes of vibrations and linkages present in the prepared glass samples. Moreover, the Monte Carlo simulation was used to estimate the radiation shielding properties of the PbCKNP glass system. The highest LAC achieved for the fabricated glass sample PbCKNP5 decreased in the range between 159.07 and 0.123 cm⁻¹ with increasing the gamma photon energy between 0.015 and 15 MeV. The substitution of the Na₂O by PbO in the fabricated glass system positively affects the LAC values. Thus, the fabricated glass PbCKNP5 with 20 mol% of PbO content has the best photon shielding parameters among the studied glasses.

Acknowledgments

We would like to thank Taif University Researchers Supporting Project Number (TURSP-2020/226), Taif University, Taif, Saudi Arabia for financial support.

References

1. F.O. Ogundare, I.O. Olarinoye, R.I. Obed, Estimation of patients' organ doses and conceptus doses from selected X-ray examinations in two Nigeria X-ray centers. *Radiat. Prot. Dosimetry.* **132**(4), 395–402 (2008). <https://doi.org/10.1093/rpd/ncn317>
2. F.O. Ogundare, I.O. Olarinoye, He⁺ induced changes in the surface structure and optical properties of RF-sputtered amorphous alumina thin films. *J. Non Crystalline Solids* **432**, 292–299 (2016). <https://doi.org/10.1016/j.jnoncrysol.2015.10.026>
3. E. Gölge, G. Ova, The effects of food irradiation on quality of pine nut kernels. *Radiat. Phys. Chem.* (2008). <https://doi.org/10.1016/j.radphyschem.2007.06.005>
4. E. Gölge, G. Ova, The effects of food irradiation on quality of pine nut kernels. *Radiat. Phys. Chem.* (2008). <https://doi.org/10.1016/j.radphyschem.2007.06.005>
5. X.B. Wang, C.N. Wang, Y.C. Zhang, T.T. Liu, J.P. Lv, X. Shen et al., Effects of gamma radiation on microbial, physicochemical, and structural properties of whey protein model system. *J. Dairy Sci.* (2018). <https://doi.org/10.3168/jds.2017-14085>
6. S. Matsunaga, T. Shuto, N. Kawahara, J. Suenaga, S. Inomori, H. Fujino, Gamma Knife surgery for brain metastases from colorectal cancer. *J. Neurosurg.* **114**, 782–789 (2011). <http://doi.org/10.3171/2010.9.JNS10354>
7. Y. Kavun, I. Boztosun, H. Dapo, I. Maraş, C. Segebade, Determination of the Sr/Ca ratio of tooth samples, by photoactivation analysis in Southern Turkey. *Radiochim Acta* (2018). <https://doi.org/10.1515/ract-2017-2918>
8. O. Olarinoye, C. Oche, Gamma-rays and fast neutrons shielding parameters of two new Ti-based bulk metallic glasses. *Iran. J. Med. Phys.* (2020). <https://doi.org/10.22038/ijmp.2020.42684.1635>
9. M.I. Sayyed, K.A. Mahmoud, O.L. Tashlykov, M.U. Khadaker, M.R.I. Faruque, Enhancement of the shielding capability of soda-lime glasses with Sb₂O₃ Dopant: a potential material for radiation safety in nuclear installations. *Appl. Sci.* **11**, 326 (2021). <https://doi.org/10.3390/app11010326>
10. M.I. Sayyed, M.H.A. Mhareb, Y.S.M. Alajerami, K.A. Mahmoud, M.A. Imheidat, F. Alshahri, M. Alqhtani, T. Al-Abdullah, Optical and radiation shielding features for a new series of borate glass samples. *Optik* **239**, 166790 (2021)
11. Y.S. Rammah, I.O. Olarinoye, F.I. El-Agawany, A. El-Adawy, El Sayed Yousef. The f-factor, neutron, gamma radiation and proton shielding competences of glasses with Pb or Pb/Bi heavy elements for nuclear protection applications. *Ceram. Int.* **46**, 27163–27174. <https://doi.org/10.1016/j.ceramint.2020.07.197>
12. M.I. Sayyed, K.A. Mahmoud, E. Lacomme, M.M. AlShammari, Y.S.M. Nidal Dwaikat, M. Alajerami, B.O. Alqhtani, M.H.A. El-bashir, Mhareb, 2021. Development of a novel MoO₃-doped borate glass network for gamma-ray shielding applications, *Eur. Phys. J. Plus* (2021) 136:108 <https://doi.org/10.1140/epjp/s13360-020-01011-5>
13. G. Lakshminarayana, MG Dong, Ashok Kumar, Y Elmahroug, Akshatha Wagh, Dong-Eun Lee, Jonghun Yoon, Taejoon Park, “Assessment of gamma-rays and fast neutron beam attenuation features of Er₂O₃-doped B₂O₃-ZnO-Bi₂O₃

- glasses using XCOM and simulation codes (MCNP5 and Geant4)” *Applied Physics A* **125** (2019) 1–14.
14. AM Ali, MI Sayyed, M Rashad, A Kumar, R Kaur, A Aşkın, H Algarni, “Gamma ray shielding behavior of Li₂O-doped PbO–MoO₃–B₂O₃ glass system” *Applied Physics A* **125** (2019) 671.
 15. A. Kumar, M.G. Dong, M.I. Sayyed, G. Lakshminarayana, X.X. Xue, M.A. Mahdi, “Gamma-ray shielding effectiveness of lead bismuth germanoborate glasses”. *Glass Phys. Chem.* **44**, 292–299 (2018)
 16. M.I. Sayyed, Y. Al-Hadeethi, M.M. AlShammari, S.H. Ahmed, Y.S. Al-Heniti, Rammah, Physical, optical and gamma radiation shielding competence of newly borotellurite based glasses: TeO₂–B₂O₃–ZnO–Li₂O₃–Bi₂O₃. *Ceram. Int.* **47**, 611–618 (2021)
 17. E. Metwalli, M. Karabulut, D.L. Sidebottom, M.M. Morsi, R.K. Brow, Properties and structure of copper ultraphosphate glasses. *J Non Cryst Solids* **344**, 128–134 (2004). <https://doi.org/10.1016/j.jnoncrysol.2004.07.058>
 18. U. Perişanoğlu, F.I. El-Agawany, E. Kavaz, M. Al-Buriah, Y.S. Rammah, Surveying of Na₂O₃–BaO–PbO–Nb₂O₅–SiO₂–Al₂O₃ glass-ceramics system in terms of alpha, proton, neutron and gamma protection features by utilizing GEANT4 simulation codes. *Ceram. Int.* **46**(3), 3190–3202 (2020)
 19. P. Aly, A.A. El-Kheshen, H. Abou-Gabal, S. Agamy (2020). Structural investigation and measurement of the shielding effect of borosilicate glass containing PbO, SrO, and BaO against gamma irradiation. *Journal of Physics and Chemistry of Solids*, 109521
 20. A.H. Almuqrin, M.I. Sayyed, Radiation shielding characterizations and investigation of TeO₂–WO₃–Bi₂O₃ and TeO₂–WO₃–PbO glasses. *Appl. Phys. A* **127**, 190 (2021)
 21. E. Kavaz, E.H. Ghanim, A.S. Abouhaswa, Optical, structural and nuclear radiation security properties of newly fabricated V₂O₅–SrO–PbO glass system. *J. Non-Cryst. Solids* **538**, 120045 (2020)
 22. Agar, O., Khattari, Z. Y., Sayyed, M. I., Tekin, H. O., Al-Omari, S., Maghrabi, M., et al., Evaluation of the shielding parameters of alkaline earth based phosphate glasses using MCNPX code. *Results Phys.* **12**, 101–106 (2019)
 23. A. El-Taher, A.M. Ali, Y.B. Saddeek, R. Elsaman, H. Algarni, K. Shaaban, T.Z. Amer, Gamma ray shielding and structural properties of iron alkali alumino-phosphate glasses modified by PbO. *Radiat. Phys. Chem.* **165**, 108403 (2019)
 24. S.A. Issa, M.I. Sayyed, A.M.A. Mostafa, G. Lakshminarayana, I.V. Kityk, Investigation of mechanical and radiation shielding features of heavy metal oxide based phosphate glasses for gamma radiation attenuation applications. *J. Mater. Sci.: Mater. Electron.* **30**(13), 12140–12151 (2019)
 25. Ashok Kumar, Gamma ray shielding properties of PbO–Li₂O–B₂O₃ glasses. *Radiat. Phys. Chem.* **136**, 50–53 (2017)
 26. A. Kumar, D.K. Gaikwad, S.S. Obaid, H.O. Tekin, O. Agar, M.I. Sayyed, Experimental studies and Monte carlo simulations on gamma ray shielding competence of (30 + x) PbO–10 WO₃–10Na₂O–10MgO–(40-x) B₂O₃. *Prog. Nucl. Energy* **119**, 103047 (2020)
 27. F. Laariedh, M.I. Sayyed, A. Kumar, H.O. Tekin, R. Kaur, T.-B. Badeche, Studies on the structural, optical and radiation shielding properties of (50–x) PbO–10 WO₃–10 Na₂O–10 MgO–(20 + x) B₂O₃ glasses. *J. Non-Cryst. Solids* **513**, 159–166 (2019)
 28. A. Kumar, R. Kaur, M.I. Sayyed, M. Rashad, M. Singh, A.M. Ali, “Physical, structural, optical and gamma ray shielding behavior of (20 + x) PbO – 10 BaO – 10 Na₂O – 10 MgO – (50-x) B₂O₃ glasses”. *Physica B* **552**, 110–118 (2019)
 29. X-5 Monte Carlo Team, M.C.N.P.A. General Monte Carlo N-Particle Transport Code, Version 5, Los Alamos Controlled Publication. LA-CP-03-0245 (n.d.) 2003
 30. D. Toloman, D.A. Magdas, I. Bratu, L.M. Giurgiu, k and I. Ardelean, Infrared spectra of calcium phosphate glasses. *Int J f Mod Phys B*, **24**, 351–358 (2010)
 31. L. Maria Bosca, G. Pop, P. Borodi, E. Pascuta, Culea, XRD and FTIR structural investigations of erbium-doped bismuth–lead–silver glasses and glass ceramics. *J. Alloy. Compd.* **479**, 579–582 (2009)
 32. R. Divina, G. Sathiyapriya, K. Marimuthua, A. Askin, M.I. Sayyed, Structural, elastic, optical and γ -ray shielding behavior of Dy³⁺ ions doped heavy metal incorporated borate glasses. *J. Non-Cryst. Solids* **545**, 120269 (2020)
 33. M.A. Marzouk, H.A. ElBatal, Y.M. Hamdy, F.M. Ezz-Eldin, Collective optical, FTIR, and photoluminescence spectra of CeO₂ and/or Sm₂O₃-doped Na₂O–ZnO–P₂O₅ glasses. *Int. J. Opt.* (2019) 6527327
 34. V.N. Rai, B.N. Raja Sekhar, D.M. Phase, S.K. Deb, Effect of gamma irradiation on the structure and valence state of Nd in phosphate glass. *arXiv preprint arXiv:1406.4686* (2014)
 35. Y.M. Lai, X.F. Liang, S.Y. Yang, J.X. Wang, L.H. Cao, B. Dai, Raman and FTIR spectra of iron phosphate glasses containing cerium. *J. Mol. Struct.* **992**, 84–88 (2011)

Publisher’s Note Springer Nature remains neutral with regard to jurisdictional claims in published maps and institutional affiliations.